

Theoretical Model of the Two-Chamber Pressure Casting Process

R.G. KEANINI, K. WATANABE, and T. OKABE

This article develops a theoretical model of the two-chamber pressure casting process. In this process, a molten metal drop, formed by arc melting a solid ingot, falls into a conical crucible attached to a gas-filled, porous cast mold. An energy-based formulation of the mold-filling process is developed which focuses on the drop's motion within the crucible and mold cavity and on pressure evolution within the mold cavity. The model shows that drop acceleration into the mold depends on three dimensionless parameters, the Euler number, Eu , the Froude number, Fr , and the pressure loss coefficient, K , across the crucible exit. These parameters are in turn determined by the mold's permeability to the process gas, the characteristic initial pressure difference between the interior and exterior of the mold, the mold thickness, the process gas viscosity, and the metal density. Drop acceleration into the mold compresses trapped gas within the mold cavity; under most conditions, pressure decay due to leakage of the trapped gas through the mold occurs at a faster rate than inertial compression. Under these circumstances, a downward acting pressure force, having a magnitude determined by the Euler number, acts on the drop. At low Froude numbers, however, gas compression occurs at a *faster* rate than leakage-induced decay and the pressure force acts upward, again with a magnitude determined by Eu . Scaling arguments show that friction and evaporation recoil forces are negligible in determining drop motion, while surface tension, pressure, drop inertia, and gravity are dominant. In addition, solidification effects are shown to be negligible.

I. INTRODUCTION

TITANIUM has found increasing use in dental prosthetics, principally as an alternative to allergy-producing casting alloys.^[1] Although titanium is difficult to cast using the lost-wax method,^[2] technical improvements have led to various methods for preparing acceptable clinical dental prostheses.^[2] Dental appliance casting units can be categorized as one of two types, depending on how liquid metal is forced into the cast mold: pressure difference casting units and centrifugal casting machines. This study will consider the former, focusing in particular on the two-chamber pressure casting process.

A typical two-chamber casting unit is shown schematically in Figure 1. Here, the upper and lower chambers within the casting unit are separated by an impermeable wall, which supports the cast mold. Both chambers are filled with an inert gas, typically argon, with the lower chamber pressure maintained at approximately 20 kPa ($=P_l$) and the upper chamber set at approximately 200 kPa ($=P_u$). Due to the pressure difference between the mold's interior and exterior, gas flows through the mold's porous bottom wall into the lower chamber. Casting is initiated when a titanium (or, more generally, a metal) ingot is arc melted within a copper crucible in the upper chamber; a molten drop eventually forms and falls into

the conical crucible positioned immediately above the mold cavity. Although the pressure within the upper chamber and that within the mold cavity are initially equal, once the drop falls into the crucible, the gas trapped within the mold cavity continues to pass through the porous mold into the lower chamber. Due to a combination of gas leakage from the mold cavity and compression due to the drop's downward motion, a time-dependent pressure difference, $P_u - P(t)$, is created across the molten drop.

Considering the dynamics of the drop, it is apparent that at least two forces drive the molten metal into the mold cavity: the weight of the metal itself and the time-varying pressure difference that develops across the melt. Other forces that potentially play a role in cast filling dynamics include surface tension, impulse due to metal evaporation, and friction. Each of these will be discussed subsequently. With regard to the pressure force, once a molten drop falls into the conical crucible above the mold cavity, the drop's upper free surface is subject to the relatively fixed pressure, P_u , within the upper chamber, while the drop's lower free surface is subject to a time varying pressure, $P(t)$, within the mold cavity. The cavity pressure depends principally on the rate of process gas loss from the cavity, which in turn depends on the mold's permeability, k_g ,^[5-8] the gas viscosity, μ_g , the mold's thickness, t_d , the surface area within the mold cavity available for porous gas transport, A_c , and the pressure difference, $P(t) - P_l$, across the mold wall. Previous work has inappropriately identified the (fixed) pressure difference between the upper and lower chambers, $P_u - P_l$, as the dynamic feature driving metal flow into the mold cavity. In reality, the appropriate pressure difference, and one of the key dynamic features examined here, is the time-dependent pressure difference $P_u - P(t)$ across the drop.^[9,10]

Although the basic principal of operation is apparent, the physical processes underlying the two-chamber pressure

R.G. KEANINI, Associate Professor, is with the Department of Mechanical Engineering & Engineering Science, University of North Carolina at Charlotte, Charlotte, NC 28223. K. WATANABE, Associate Professor, Division of Dental Biomaterials Science, Graduate School of Medical and Dental Sciences, Niigata University, Japan, 5274 Gakkouchi-dori 2 Niigata, Japan 951-8514. T. OKABE, Regents Professor and Chairman, Department of Biomaterials Science, Baylor College of Dentistry, Texas A&M University System Health Science Center, Dallas, TX 75246.

Manuscript submitted March 29, 2004.

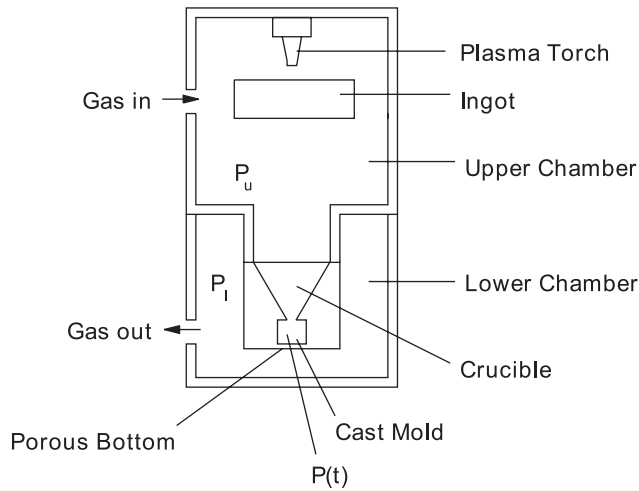


Fig. 1—Schematic of the two-chamber pressure casting process.

casting process are poorly understood. This reflects the relative complexity of the process: casting occurs rapidly, on the order of 0.1 seconds or less; the casts are small, having volumes on the order of 1 cm^3 ; process gas can be trapped within the mold cavity, leading to cast porosity;^[3,4] and solidification occurs rapidly, possibly affecting cast quality. Progress in minimizing and controlling cast nonuniformity requires improved understanding of process physics, and in particular, an improved understanding of cast metal flow and mold filling.

The purpose of this article is to theoretically investigate the two-chamber pressure casting process. We use scaling arguments to first establish the important physical features underlying the process. A simple energy-based model of drop motion and mold filling during casting is then developed. The analysis and results provide useful physical insight into the complex features underlying rapid casting of dental prostheses and should provide a framework for future studies of other dental casting processes.

II. PHYSICAL FEATURES AND SCALING ARGUMENTS

Prior to formulating a process model, we use scaling analysis^[11] to determine the essential physical features underlying the casting operation. This will provide a fuller understanding of process physics as well as a basis for developing the model.

A. Heat Transfer and Drop Solidification

In order to examine the effect of solidification on the casting process, we estimate the amount of solidification that occurs at the crucible exit during mold filling. We are particularly interested in determining if rapid solidification at this location can significantly slow or even shunt liquid metal flow into the mold. A straightforward estimate, which provides an upper bound on the solidification speed, can be obtained by assuming that the characteristic heat flux from the drop to the crucible is on the order of the flux, q_p , from

Table I. Parameter Values

Parameter	Magnitude	Reference
h_{fg}	$8.9 \times 10^6 \text{ J kg}^{-1}$	19
h_{sl}	$3.88 \times 10^5 \text{ J kg}^{-1}$	19
H_c, L_c	$1.0 \times 10^{-2} \text{ m}$	20
k_g	$1.0 \times 10^{-14} \text{ m}^2$	12
k_l, k_s	$2.19 \times 10 \text{ Wm}^{-1} \text{ }^\circ\text{C}^{-1}$	21
L_s	$2.5 \times 10^{-2} \text{ m}$	20
P_l	$2.0 \times 10^4 \text{ Pa}$	20
P_o, P_u	$2.0 \times 10^5 \text{ Pa}$	20
R_o	$2.5 \times 10^{-3} \text{ m}$	20
R_u	$1.5 \times 10^{-2} \text{ m}$	20
t_d	$7.6 \times 10^{-4} \text{ m}$	20
T_g, T_o	$2.5 \times 10 \text{ }^\circ\text{C}$	20
T_m	$1.945 \times 10^3 \text{ }^\circ\text{C}$	21
T_b	$3.56 \times 10^3 \text{ }^\circ\text{C}$	22
V_d	$7.06 \times 10^{-6} \text{ m}$	20
U_o	1.0 ms^{-1}	20
α_m	$9.22 \times 10^{-6} \text{ m}^2\text{s}^{-1}$	21
μ_g	$1.5 \times 10^{-5} \text{ Nsm}^{-2}$	22
μ_m	$1.0 \times 10^{-3} \text{ Nsm}^{-2}$	23
ρ_m	$4.54 \times 10^3 \text{ Nsm}^{-2}$	21
σ	$1.5 \times 10 \text{ N m}^{-1}$	23

the plasma torch to the ingot during melting. Expressing the energy balance across the moving solidification front, we have

$$k_l \frac{\partial T}{\partial n} + \rho_m h_{sl} U_m = k_s \frac{\partial T}{\partial n} \quad [1]$$

where k_l and k_s are the metal's liquid- and solid-phase thermal conductivities, ρ_m is the metal density, h_{sl} is the heat of fusion, \mathbf{n} is the local unit normal to the propagating solidification front (directed in the direction of front motion), and U_m is the local solidification front speed. Balancing the latent heat generation term with either of the conductive flux terms and estimating the conductive flux as q_p , we obtain

$$U_m \approx \frac{q_p}{\rho_m h_{sl}} \quad [2]$$

Given U_m , the approximate (maximum) thickness, δ_s , of the solidification front at the end of the cavity filling process is given by $\delta_s \approx U_m \tau_{\text{fill}}$, where τ_{fill} is the time required to fill the mold. Letting $\tau_{\text{fill}} \approx 10^{-1} \text{ s}$,^[12] taking $q_p = 10^6 \text{ Wm}^2$,^[13] and using the parameter values in Table I, we find that $\delta_s \approx 5.7 \times 10^{-5} \text{ m}$. Since δ_s is less than 3 pct of the crucible exit radius, it is clear that negligible solidification occurs during cavity filling and that metal flows relatively unimpeded into the mold.

B. Fluid Friction

Viscous forces between the drop and the crucible and mold walls play a negligible role in determining drop dynamics. We show this by first estimating the characteristic shear stress, τ , exerted by the crucible wall on the liquid metal:

$$\tau \approx \mu_m \frac{\partial w}{\partial n} \approx \frac{\mu_m U_o}{\delta} \quad [3]$$

where μ_m is the liquid metal's dynamic viscosity, n is a coordinate normal to the crucible wall, w is the streamwise velocity, U_o is the characteristic axial velocity within the crucible (taken as the characteristic velocity through the crucible exit), and δ is the characteristic viscous boundary layer thickness. The boundary layer thickness is estimated by balancing the dominant viscous and advective terms in the streamwise momentum equation, yielding

$$\delta \approx \sqrt{\frac{v_m L_s}{U_o}} \quad [4]$$

where v_m is the kinematic viscosity and L_s is the crucible's axial length. Thus, the approximate frictional force retarding drop motion into the cast is $F_f \approx \tau A_{sp}$, where A_{sp} is the characteristic crucible area contacted by the drop; using parameter values listed in Table I, we find that $F_f \approx 0.018 \text{ N}$. Next, we estimate the net pressure force across the drop as $(P_u - P_c)A_o$, where P_c is the characteristic pressure acting on the drop's lower free surface, and A_o is the area of the crucible exit. (This estimate follows by first recognizing that the characteristic upward-acting reaction force exerted on the drop by the crucible's lateral walls, $P_u(A_u - A_o)$, largely offsets the characteristic downward pressure force, $P_u A_u$, acting on the drop's upper free surface (Section III–G) Second, the characteristic downward reaction force exerted on the drop by the mold cavity's upper wall, $P_c(A_c - A_o)$, essentially offsets the characteristic upward pressure force, $P_c A_c$, acting on the drop's lower free surface. Here, A_u and A_c are the cross-sectional areas at the top of the crucible and within the mold cavity. A force balance on the drop then leads to the given estimate. Thus, it is found that friction is of negligible importance when the characteristic pressure force across the drop, $(P_u - P_c)A_o$, is larger than 0.018 N ($\approx F_f$), a condition that holds essentially throughout the filling process (based on inspection of the computed results discussed subsequently).

Considering briefly the contribution of viscous dissipation to the drop's thermal energy balance, it is likewise readily shown that frictional heating, limited to viscous boundary layers near each solid surface, is of negligible importance.

C. Surface Tension–Surface Potential Energy

A quality cast requires that the drop maintain its integrity against external pressure forces during casting. This in turn requires that surface tension forces are comparable to the pressure forces. We can show that this condition generally holds by comparing characteristic surface tension forces on the drop's upper and lower free surfaces against the characteristic pressure force across the drop. The upward-acting surface tension force within the crucible, F_{STu} , is estimated as $F_{STu} \approx \sigma 2\pi R_u \cos(\phi)$, where R_u is the crucible's upper radius, ϕ ($=26.5 \text{ deg}$) is the conical crucible's half angle, σ is the surface tension coefficient, and where the contact angle between the liquid metal and crucible is assumed to be approximately 0. Similarly, the downward acting force, F_{STl} , on the lower free surface is $F_{STl} \approx 4\sigma L_c$, where L_c is the length of each of the square cavity's sides. Thus, we find that surface tension forces are comparable to pressure forces when the characteristic pressure difference across the drop satisfies $\Delta P = P_u - P_c \leq F_{ST}/A_o \approx 64 \text{ kPa}$, a condition that

typically holds over a large portion of the filling process. (Here, F_{ST} represents either F_{STu} or F_{STl}).

While surface tension forces are comparable to pressure forces, their principal effect is to maintain the drop's free surfaces against pressure, gravity, and inertial forces. In contrast, temporal variations in the drop's surface potential energy play a negligible role in the drop's energy budget. This is shown by comparing the *maximum* rate of surface potential energy change with the characteristic rate of work done by pressure forces:

$$\frac{\frac{d}{dt} \int_A \sigma dA}{\int_A^{-A} P_u \cdot ndA} \approx \frac{\sigma \frac{Au}{\tau_{fill}}}{P_u U_u A_u}$$

Based on the parameter values given in Table I, we find that this ratio is approximately 0.03, showing that surface potential energy variations are of secondary importance. Here, U_u is the characteristic velocity of the drop's upper free surface and $U_u A_u = U_o A_o$ (from continuity).

D. Evaporation Recoil

Due to the drop's relatively high temperature, the momentum flux due to evaporation from either free surface (evaporation recoil) can be significant. The characteristic rate of metal evaporation \dot{m}_e is given by $\dot{m}_e = \rho_e v_e A_e = \dot{Q} h_{fg}$, where ρ_e and v_e are the metal evaporate's density and velocity, A_e is the evaporating surface area, \dot{Q} is the characteristic rate of heat transfer from the drop's interior to the evaporating surface, and h_{fg} is the metal's latent heat of vaporization. Given the evaporate velocity, the approximate recoil force, F_e , can be estimated as $F_e = \rho_e v_e^2 A_e$. In order to estimate ρ_e , we note that evaporate particles thermally equilibrate with the surrounding process gas within one electron mean free path of the evaporating surface.^[13] Thus,

$$\rho_e = \frac{P_o}{RT_o}$$

where P_o and T_o are the ambient pressure and temperature of the process gas, and R is the gas constant for titanium. Taking \dot{Q} as being on the order of $q_p A_e \approx q_p A_u$, which again likely represents an overestimate, and using the parameter values in Table I, we find that $F_e \approx 2 \times 10^{-6} \text{ N}$. Since this is again several orders of magnitude smaller than the characteristic pressure force acting across the drop, $(P_u - P_c)A_o$, evaporation recoil plays a negligible role in cast filling dynamics.

E. Mold Gas Flow and Gas Heating during Filling

The model developed subsequently assumes that argon within the mold cavity remains isothermal during the filling process. This assumption is valid if the characteristic thermal diffusion time, τ_d , for gas within the cavity is much longer than the cavity fill time, τ_{fill} . Although significant gas flow may be induced as the liquid metal flows into the cavity, it is not expected that significant convective heat transfer occurs within the gas. Specifically, gas motion will likely assume a form somewhere between one of two extremes: (1) for a highly permeable bottom wall, gas motion will be

largely uniaxial and directed toward the bottom; and (2) for a slightly or a moderately permeable bottom, gas motion will be largely laminar and circulatory. In the first case, it is clear that since minimal convective mixing occurs, in-gas heat transfer will be conduction dominated. In the latter case, since the metal drop's lower free surface remains smooth (Section III–G) and since the cavity walls are also smooth, no apparent mechanism exists for creating strong convective mixing within recirculating gas pockets. Thus, again, gas heat transfer is largely determined by conduction. Comparing the diffusive time scale, given by $\tau_d \approx L_c^2/\alpha_a$, where α_a is argon's thermal diffusivity, with a characteristic fill time of $\tau_{\text{fill}} (\approx 0.1 \text{ s}^{[11]})$, we find that $\tau_d/\tau_{\text{fill}} = O(10^2)$, showing that the isothermal gas approximation is valid.

F. Gas Flow through Cavity Wall

As molten metal flows into the mold cavity, process gas trapped within the cavity quickly leaks through the cavity's porous bottom (into the surrounding lower chamber). Assuming that the bottom's porosity is isotropic, gas transport through the wall is governed by Darcy's law:

$$\mathbf{v} = -\frac{k_g}{\mu_g} \nabla P \quad [5]$$

where \mathbf{v} is the local gas velocity, k_g is the gas permeability, μ_g is the gas viscosity, and P is the local pressure.

G. Free Surface Curvature and Rayleigh–Taylor Instability

The model developed subsequently assumes that the drop's upper and lower capillary surfaces remain flat throughout the filling process. We can estimate the characteristic curvature of the drop's free surfaces using the Young–Laplace equation:

$$P_\alpha - P_i = \sigma \nabla_H \cdot \mathbf{n} \quad [6]$$

where P_α denotes local external pressure at the upper (P_u) or lower (P) interface, P_i is the corresponding interfacial pressure within the drop, \mathbf{n} is the local outward unit normal to the interface, and $\nabla_H = e_x - e_x \frac{\delta}{\delta x} + e_y \frac{\delta}{\delta y}$ is the surface divergence operator. The characteristic surface curvature, $R_s^{-1} (\approx \nabla_H \cdot \mathbf{n})$, can be estimated using the characteristic pressure difference, ΔP_s , across either interface:

$$\nabla_H \cdot \mathbf{n} \approx R_s^{-1} \approx \frac{\Delta P_s}{\sigma} \quad [7]$$

Considering first the upper interface (within the crucible), since flow within the crucible is largely inviscid (discussed subsequently), the pressure variation, ΔP_s , between the upper surface and crucible exit can be estimated via Bernoulli's equation as $\Delta P_s \approx \rho_m U_o^2 \approx 5 \times 10^3 \text{ N m}^{-2}$ (where the hydrostatic contribution, $\rho_m g L_s \approx 10^3 \text{ N m}^{-2}$, is of the same order). Thus, since the upper chamber pressure P_u is nearly two orders of magnitude larger, metal within the crucible remains essentially isobaric at the upper chamber pressure.

From Reference 7, it is clear then that curvature is small. (Note, since drop volumes are larger than the mold cavity volume, the drop's upper surface remains within the crucible throughout the filling process.)

Considering the lower interface, we are confronted with the problem of estimating pressure loss across the crucible exit. Large pressure losses lead to relatively flat lower free surfaces, while small pressure losses lead to large surface curvature, particularly as cavity pressure decays. Since pressure loss is unknown, we note indirect evidence that lower surface curvature remains small, *i.e.*, significantly smaller than the inverse cavity width, L_c^{-1} : if the curvature was large, *i.e.*, on the order of L_c^{-1} , then the drop would quickly impinge and cover the lower porous boundary. Process gas would then be trapped, leading to significant cast porosity. Since porosity is generally small, however, premature impingement appears unlikely, suggesting that the lower interface remains relatively flat.

Considering next the lower free surface's stability, since a high density fluid (liquid metal) overlies a low density fluid (process gas), the surface may be subject to Rayleigh–Taylor capillary instability.^[14] Here, disturbances on the free surface remain stable for wavelengths shorter than a critical wavelength, λ_c , given by

$$\lambda_c = 2\pi \left[\frac{\sigma}{g(\rho_m - \rho_g)} \right]^{1/2} \quad [8]$$

where ρ_g is the gas density. Using the parameters in Table I, we find that $\lambda_c \approx 11 \text{ cm}$, which is significantly larger the largest (diagonal) dimension within the cavity. Thus, the interface remains stable during cast filling.

H. Flow Characteristics

Each metal drop is formed by melting metal ingot with a plasma torch. Due to high torch heat fluxes (on the order of 10^6 W m^{-2}), metal surface temperatures approach the metal's boiling point and thermocapillary stresses produced by surface temperature gradients become negligible. Although plasma flow over the drop drives flow within the drop, this flow is likely confined to near surface boundary layers.^[15] This is due to low liquid metal kinematic viscosity and the low viscosity of typical process plasmas. Thus, flow within the drop prior to impingement on the crucible is largely inviscid. As the drop falls into the conical crucible (where the cone's interior half-angle is approximately 26.5 deg), it impinges on the sides of the crucible and on the relatively small exit hole at the bottom of the crucible (where the ratio of the crucible's exit to entrance areas is approximately 1/36). However, based on previous work,^[16] it is expected that generation and mixing of vorticity during impingement will not significantly alter the inviscid nature of drop flow. Thus, flow within the drop appears to remain inviscid as it falls into the crucible and fills the mold.

III. PROCESS MODEL

Based on the physical considerations discussed in Section III, we can now formulate a relatively simple energy-based model of liquid metal motion within the crucible and mold

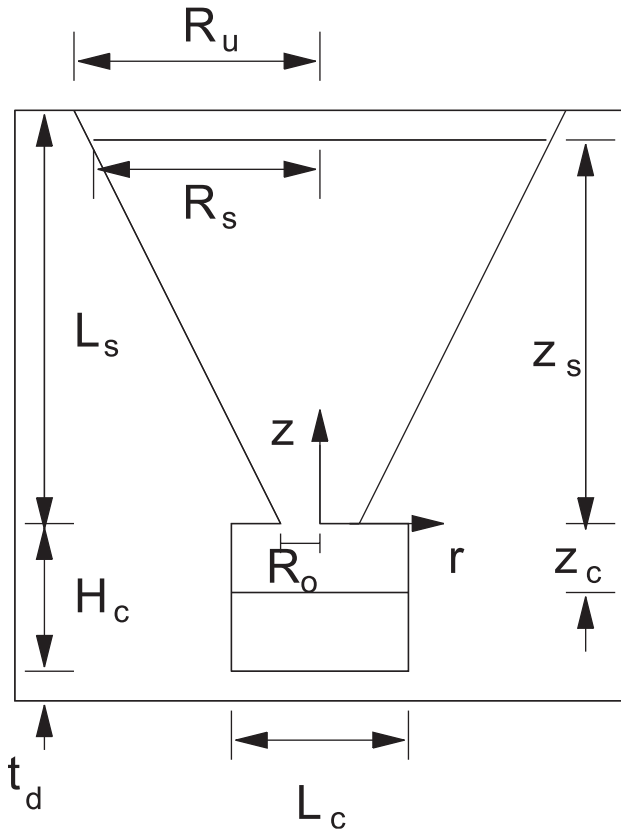


Fig. 2—Process variables and dimensions.

during mold filling. A detailed sketch of the process is shown in Figure 2. The instantaneous mechanical energy balance for fluid within the crucible is given by

$$\frac{d}{dt} \int_{V_s} \frac{\rho}{2} \mathbf{u} \cdot \mathbf{u} dV = - \int_{A_o^+} \frac{\rho}{2} (\mathbf{u} \cdot \mathbf{u}) \mathbf{u} \cdot \mathbf{n} dS - \int_{A_o} \rho \left(\frac{P}{\rho} + gz \right) \mathbf{u} \cdot \mathbf{n} dS \quad [9]$$

where $V_s = V_s(t)$ is the volume of liquid metal within the crucible, \mathbf{u} is the liquid metal velocity field, P is the associated pressure field, A_o^+ is the area of the crucible's exit, $A_s = A_s(t)$ is the liquid metal's upper free surface area (within the crucible), and \mathbf{n} is the outward unit normal on either A_o^+ or A_s . (Note that A_o^+ is located at $z = 0^+$; this allows an unambiguous derivation of the overall energy balance given subsequently. Note too that in the following, we suppress the subscript on the liquid metal density, ρ_m .) A similar expression can be written for liquid metal within the mold cavity:

$$\frac{d}{dt} \int_{V_c} \frac{\rho}{2} \mathbf{u} \cdot \mathbf{u} dV = - \int_{A_o^-} \frac{\rho}{2} (\mathbf{u} \cdot \mathbf{u}) \mathbf{u} \cdot \mathbf{n} dS - \int_{A_c} \rho \left(\frac{P}{\rho} + gz \right) \mathbf{u} \cdot \mathbf{n} dS \quad [10]$$

where $V_c = V_c(t)$ is the liquid metal volume within the mold, $A_o^- = A_o^+ = A_o$ is the crucible exit area (evaluated at $z = 0^-$), and A_c is the liquid metal's lower free surface within the mold. Note that the gravitational work terms in Eqs. [9] and [10] anticipate use of a one-dimensional (1-D) flow approximation

on the upper and lower free surfaces. Adding Eqs. [9] and [10], we obtain the overall instantaneous mechanical energy balance on the metal drop:

$$\frac{d}{dt} \int_{V_d} \rho \frac{1}{2} \mathbf{u} \cdot \mathbf{u} dV = - \int_{A_d} \rho \frac{1}{2} (\mathbf{u} \cdot \mathbf{u}) \mathbf{u} \cdot \mathbf{n} dS - \int_{A_d} \rho \left(\frac{P}{\rho} + gz \right) \mathbf{u} \cdot \mathbf{n} dS - \int_{A_o} (P^+ - P^-) \mathbf{u} \cdot \mathbf{n} dS \quad [11]$$

where V_d is the (constant) total liquid metal drop volume, A_d is the drop's total free surface area, and P^+ and P^- are the pressures at $z = 0^+$ and $z = 0^-$, respectively.

We define the following area-averaged properties

$$\bar{P} = Q^{-1} \int_A P \mathbf{u} \cdot \mathbf{n} dS \quad \bar{z} = Q^{-1} \int_A z \mathbf{u} \cdot \mathbf{n} dS$$

$$\bar{U}^2 = Q^{-1} \int_A (\mathbf{u} \cdot \mathbf{u}) \mathbf{u} \cdot \mathbf{n} dS$$

where $Q = \int_A \mathbf{u} \cdot \mathbf{n} dS$ is the volumetric flow rate through area A , and defining a loss coefficient,^[17] K , as

$$\bar{P}^+ - \bar{P} = K \frac{\rho \bar{U}^2}{2} \quad [12]$$

we can express [11] as

$$\int_{V_d} \rho \frac{1}{2} \frac{\partial}{\partial t} U^2 dV = \dot{m} \left[\frac{\bar{P}_s - \bar{P}_c}{\rho} + g(\bar{z}_s - \bar{z}_c) + \frac{1}{2} (\bar{U}_s^2 - \bar{U}_c^2) - K \frac{\bar{U}_o^2}{2} \right] \quad [13]$$

where the Liebnitz rule and divergence theorem have been used, and where $U^2 = \mathbf{u} \cdot \mathbf{u}$ and $\bar{U}_o^2 = \bar{U}^2$ at the crucible exit.

In order to evaluate the volume integral in Eq. [13], we assume that the velocity distribution at any axial position z within the crucible and cavity is 1-D and is directed in the axial direction. As discussed previously, flow within the crucible is largely inviscid. Since it is expected that the velocity field within the crucible approaches three-dimensional potential flow into a mass sink (located at the crucible's apparent vertex), an estimate of the error associated with the 1-D flow assumption can be obtained by calculating the ratio, α , of the kinetic energy flux due to potential sink flow against that due to 1-D parallel flow:

$$\alpha = (\pi R^2(z))^1 \int \int \int \left(\frac{u_r^2 + u_z^2}{U^2} \right) r^2 \sin \phi d\theta d\phi dr \quad [14]$$

where u_r and u_z are the radial and axial velocity components for sink flow and where the integration is carried out over the crucible's cross-sectional area at any position z . The calculation shows that $\alpha = 1.19$. Thus, due to the relative steepness of the crucible's conical wall, the 1-D flow assumption is reasonable. Within the mold cavity, a short period of lateral spreading occurs when the metal first enters the cavity and spreads to meet the mold's vertical walls. After this, cavity flow is predominantly 1-D in the axial direction. Based on the flat free surface assumption described previously, the uniform flow approximation also appears to be reasonable within the mold cavity.

The volume integral in Eq. [13] thus becomes

$$\int_{V_d} \frac{\rho}{2} \frac{\partial U^2}{\partial t} dV = \frac{\rho}{2A_c^2} \int_{V_c} \frac{d}{dt} [\dot{z}_s(mz_s + R_o)^2 \pi]^2 dz + \frac{\rho}{2} \int_{V_s} \frac{d}{dt} [\dot{z}_s(mz_s + R_o)^2 \pi]^2 dz \quad [15]$$

where the first integral is taken over the volume of liquid metal within the mold cavity, V_c , while the second is over the liquid metal volume within the crucible (V_s). The argument in the first integral follows by application of continuity between the metal drop's upper free surface and any axial position z occupied by liquid metal within the cavity: $\dot{z}_c L_c^2 = \dot{z}_s \pi R_s^2$, where $L_c^2 = A_c$ is the cavity's cross-sectional area, and πR_s^2 is the upper free surface's cross-sectional area (evaluated at $z = z_s$). Note that $R_s = R_s(z_s) = mz_s + R_o$, where m ($=0.5$) is the conical crucible's slope and R_o is the radius at the crucible exit. The second integral follows in a similar manner. (For clarity, we have dropped overbars on the average positions, z_s and z_c , of the upper and lower free surfaces.) Carrying out the integrations in Eq. [15] and rearranging then leads to the equation governing drop motion:

$$\int_{V_d} \rho \frac{1}{2} \frac{\partial}{\partial t} U^2 dV = -\frac{\rho \dot{z}_s A_s z_c}{A_c} [\dot{z}_s A_s + 2\pi R_s m z_s^2] + \frac{\rho \dot{z}_s \ddot{z}_s A_s^2}{m\pi} [R_o^{-1} - R_s^{-1}] \quad [16]$$

where $A_s = \pi R_s^2$.

A. Mold Gas Pressure

We assume that the process gas is argon and that it behaves as an ideal gas. The rate of gas loss from the mold cavity is given by

$$\dot{m}_g = \frac{1}{RT_g} \frac{d}{dt} (PV) \quad [17]$$

where R is the gas constant for argon, T_g is the constant gas temperature, and $P = P(t)$ and $V = V(t)$ are the time-dependent gas pressure and volume within the cavity, respectively. Since gas loss occurs due to flow through the cavity's porous bottom wall, we can also express the rate of mass loss as

$$\dot{m}_g = \int_{A_c} \rho_g \mathbf{v}_g \cdot \mathbf{n} dA = \int_{A_c} -\rho_g \frac{k_g}{\mu_g} \nabla P \cdot \mathbf{n} dA \quad [18]$$

Neglecting small spatial pressure variations due to gas flow within both the cavity and lower chamber and assuming that the bottom wall is of constant thickness, t_d , then

$$\nabla P \cdot \mathbf{n} = \frac{P - P_l}{t_d} \quad [19]$$

where again P_l is the lower chamber pressure. Note, since pressures on both sides of the bottom wall are spatially uniform, the pressure field within the wall depends only on the axial coordinate z and is governed by $d^2 P/dz^2 = 0$. Integrating this expression shows that the preceding derivative

is exact. Now, since P is spatially uniform within the cavity, the integral in Eq. [18] can be evaluated as

$$\int_S \rho_g \frac{k_g}{\mu_g} \nabla P \cdot \mathbf{n} dA = \frac{k_g A_c}{\mu_g t_d RT_g} P (P - P_l) \quad [20]$$

where the ideal gas law has been used to express ρ_g in terms of P and T_g . Setting Eqs. [17] and [18] equal to one another and substituting Eq. [20] for [18] yields

$$V\dot{P} + P\dot{V} = \frac{k_g A_c}{\mu_g t_d} P (P - P_l) \quad [21]$$

where $\dot{P} = \frac{dP}{dt}$ and $\dot{V} = \frac{dV}{dt}$.

The time rate of change of gas volume within the cavity is related to the instantaneous speed of the molten drop's lower boundary, \dot{z}_c , as follows:

$$\dot{V} = A_c \dot{z}_c \quad [22]$$

where $V(t) = (H_c + z_c)A_c$, and H_c is the cavity's height. (Note that $z_c \leq 0$.) This proves convenient when expressing z_c in terms of the drop's upper free surface position, z_s , using

$$V_d = -A_c z_c + \frac{\pi}{3m} [(mz_s + R_o)^3 + R_o^3] \quad [23]$$

where again V_d is the drop's fixed volume. Thus, substituting Eq. [22] into [21], we obtain the equation describing pressure evolution within the mold cavity:

$$\dot{P} = -\frac{1}{H_c + z_c} \left[\frac{k_g}{\mu_g t_d} P (P - P_l) + P \dot{z}_c \right] \quad [24]$$

where z_c is related to z_s through Eq. [23].

Notice from Eq. [24] that mold pressure evolution is determined by two competing processes: pressure decay due to gas leakage from the bottom of the mold (represented by the first term on the right) and compression due to the pistonlike motion of the liquid metal into the cavity (represented by the second term). Thus, if the magnitude of liquid metal's downward (negative) velocity \dot{z}_c is large enough to overcome decay due to leakage, trapped gas can be compressed, leading to increasing pressure, P .

B. Nondimensional equations

Equations [13] and [24] represent two coupled equations governing drop motion during mold filling and cavity pressure evolution. In order to obtain a fuller qualitative understanding of the process as well as to facilitate the numerical solution, Eqs. [24] and [13] are nondimensionalized as follows: (1) all lengths are scaled using the cavity width L_c (which is on the order of both the cavity height H_c and the crucible length L_s); (2) pressures are scaled using the pressure difference ΔP between the upper and lower chambers, $\Delta P = P_u - P_l$; (3) the time scale, τ_o , is chosen as the characteristic mold fill time, $\tau_o = V_m/Q_o$, where $V_m = H_c L_c^2$ is the cavity volume and Q_o is the metal's characteristic volumetric flow rate into the cavity. In order to estimate Q_o , we

recognize that this quantity is determined by the gas's characteristic rate of flow through the mold, $Q_o \approx k_g \Delta P L_c^2 \mu_g^{-1} t_d^{-1}$. Thus, τ_o is given by

$$\tau_o = \frac{\tau_d H_c \mu_g}{\Delta P k_g} \quad [25]$$

The resulting nondimensional forms of Eqs. [24] and [11] are given by

$$\dot{\tilde{P}} = -\frac{1}{1 + \tilde{z}_c} [\tilde{P} (\tilde{P}\tilde{P}) + \dot{\tilde{z}}_c] \quad [26]$$

and

$$\ddot{\tilde{z}}_s = \frac{\left[\frac{\tilde{z}_c \tilde{z}_s^2 2 \times \ddot{m}_s m}{\tilde{A}_c} + \frac{1}{2} (\tilde{z}_s \tilde{z}_c)^2 + \text{Fr}^1 (\tilde{z}_s \tilde{z}_c) + \text{Eu} (\tilde{P}_u - \tilde{P}) - K \frac{1}{2} \left(\frac{\tilde{R}_s}{\tilde{R}_o} \right)^4 \right]}{\left[\left[\tilde{R}_o^{-1} - \tilde{R}_s^{-1} \right] \frac{\tilde{A}_s}{\ddot{m}_s \pi} - \frac{\tilde{z}_c \tilde{A}_s}{\tilde{A}_c} \right]} \quad [27]$$

where $\tilde{P} = P \Delta P^{-1}$, $\tilde{z}_s = z_s L_c^{-1}$, $\tilde{z}_c = z_c L_c^{-1}$, $\tilde{P}_l = P_l \Delta P^{-1}$, $\tilde{R}_s = R_s L_c^{-1}$, $\tilde{R}_o = R_o L_c^{-1}$, $\tilde{A}_s = A_s L_c^{-2}$, and $\tilde{A}_c = A_c L_c^{-2}$.

Three dimensionless parameters, the Euler number, Eu, the Froude number, Fr, and the loss coefficient K , appear in Eq. [27] and are defined as follows:

$$\text{Eu} = \frac{\tau_o^2 \Delta P}{L_c^2 \rho_m} = \frac{t_d^2 \mu_g^2 H_c^2}{\Delta P k_g^2 \rho_m L_c^2} \quad [28]$$

$$\text{Fr} = \frac{L_c}{\tau_o g} = \frac{\Delta P^2 k_g^2 L_c}{t_d^2 H_c^2 \mu_g^2 g} \quad [29]$$

where the definition of τ_o has been used. The Euler number indicates the relative importance of pressure forces to inertia, while the Froude number indicates the relative importance of inertia to gravity forces. In interpreting the results presented in the next section, it proves useful to recognize the physical meaning of the last three terms in Eq. [27]. The term $\text{Fr}^{-1} (\tilde{z}_s - \tilde{z}_c)$ determines the drop's downward acceleration (embodied in $\ddot{\tilde{z}}_s$) due to gravity. From the definition of Fr in Eq. [29], it is seen that drop inertia is determined by the pressure difference, ΔP , mold permeability and thickness, gas viscosity, and since $H_c \approx L_c$, mold depth. If gravity is significantly larger than inertia, $\text{Fr} \ll 1$, and as shown in Section V, downward acceleration can be rapid enough for compression to overtake leakage-induced decay, causing cavity pressure to increase. The term $\text{Eu} (P_u - P)$ determines drop acceleration due to the pressure difference across the drop's upper and lower free surfaces. Under most circumstances, when compression lags, pressure decay, $P_u - P$, is positive and the drop is accelerated downward. However, when acceleration is rapid enough for compression to dominate decay, $P_u - P$ is negative and the pressure force acts upward, retarding downward acceleration. Finally, the term $K (R_s/R_o)^4$ always acts to retard the drop's downward acceleration, with a magnitude that depends on K .

IV. RESULTS AND DISCUSSION

In this section, we examine the effects of the Euler and Froude numbers and the loss coefficient and mold cross-sectional area on mold filling dynamics and mold pressure evolution. The dimensionless Eqs. [26] and [27] are solved using fourth-order Runge–Kutta integration. Initial conditions are defined as follows. The metal drop is assumed to fill the crucible, so that $\tilde{z}_u(0) = 2.5$. In addition, it is assumed that the drop's upper surface is initially stationary, or $\sim \tilde{z}_s(0) = 0$. Assuming that the drop falls a distance h_o (≈ 0.1 m) into the crucible after melting from the ingot, the approximate initial speed of liquid through the crucible exit is $\sim 2gh_o$ (≈ 1.4 ms⁻¹, neglecting the retarding effects of surface tension and gas compression within the mold). Thus, by continuity, $\sim \tilde{z}_s(0) \approx 10^{-2}$, indicating the validity of the stationary initial condition. Finally, the initial cavity pressure is set equal to the upper chamber pressure: $\tilde{P}(0) = \tilde{P}_u = 1.111$.

Reference values for the Euler and Froude numbers are determined using the nominal parameter values in Table I, giving $\text{Eu} = 1590$ and $\text{Fr} = 0.254$. A reference value for the loss coefficient can be estimated by balancing mass, linear momentum, and mechanical energy between the crucible's exit plane ($z = 0$) and an arbitrary downstream location within the mold.^[17] The result is given by

$$K = \left(1 - \frac{A_o}{A_c}\right)^2 \quad [30]$$

Since the ratio of crucible exit area to mold cross-sectional area $A_o/A_c \approx 0.196$, the reference value for K was taken as $K = 0.646$. Finally, a reference value of the mold's cross-sectional area was chosen as $A_c = 10^{-4}$ m².

Mold filling dynamics will be characterized by the dimensional time required to fill the mold, t_f (which we will refer to as the mold fill time), while mold pressure evolution will be characterized by the final dimensionless mold pressure, \tilde{P}_f , *i.e.*, the dimensionless pressure extant at the instant when liquid metal completely fills the mold. Process behavior will be investigated over the following ranges of Fr, Eu, K , and \tilde{A}_c : $10^{-2} \leq \text{Fr} \leq 10^{-2}$, $1 \leq \text{Eu} \leq 10^3$, $1 \leq K \leq 10^4$, and $1 \leq \tilde{A}_c \leq 7$.

The effect of varying Euler and Froude numbers on final mold pressure and casting time are shown in Figures 3 and 4, respectively. At low Froude numbers ($\text{Fr} \leq \approx 10^{-1/2}$), P_f is actually *higher* than the initial mold pressure of 1.11. As mentioned, from the energy and pressure evolution, Eqs. [27] and [26], when Fr^{-1} is large, downward drop acceleration, represented by $\ddot{\tilde{z}}_s$, becomes large enough for compression to overtake pressure decay due to leakage; in this case, pressure increases. Similarly, at fixed Fr less than $\approx 10^{-1/2}$, final mold pressure *increases* with decreasing Eu. In this case, since $P_u - P$ is negative, the pressure force acts upward and resistance to downward motion becomes smaller with decreasing Eu; compression and associated final mold pressure thus increase. When Fr is greater than approximately $10^{-1/2}$, the gravitational acceleration term becomes comparable to (and, at larger Fr, smaller than) the pressure-driven acceleration term. Since all terms on the right side of Eq. [26] are initially small, initial downward acceleration is likewise small, and inspection of the time-dependent mold pressure shows that compression does not overcome decay due to gas leakage.

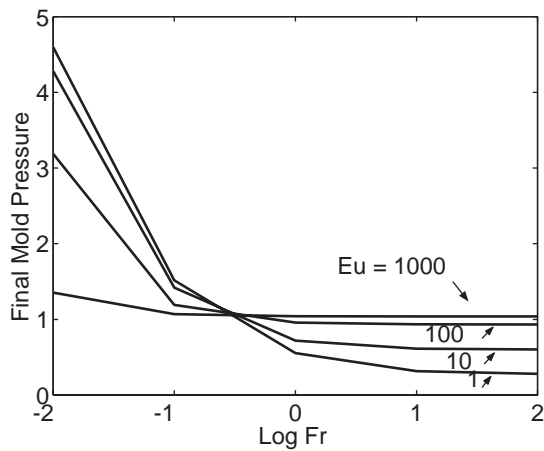


Fig. 3—Effect of Froude and Euler numbers on final dimensionless mold pressure. $K = 0.646$, $A_c = 10^{-4} \text{ m}^2$.

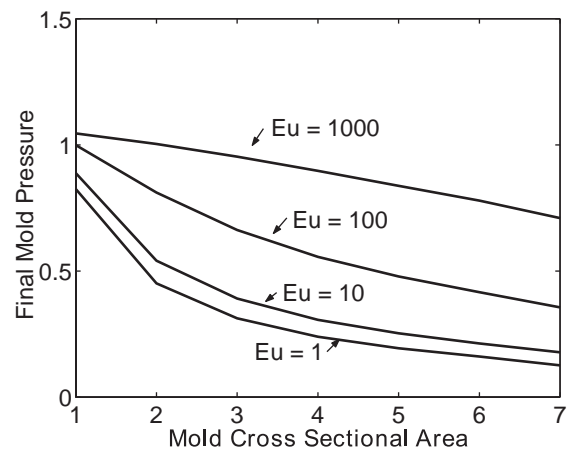


Fig. 5—Effect of dimensionless mold cross-sectional area on final dimensionless mold pressure. $K = 0.646$, $Fr = 0.254$.

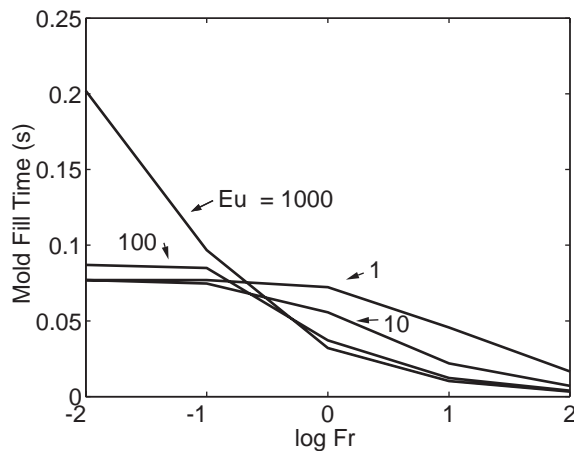


Fig. 4—Effect of Froude and Euler numbers on dimensional mold fill time. $K = 0.646$, $A_c = 10^{-4} \text{ m}^2$.

In contrast to conditions extant under small Froude numbers ($Fr < \approx 10^{-1/2}$), the pressure force thus acts downward, with a magnitude that increases with increasing Euler number. Thus, at fixed Fr and increasing Eu , pressure decay is increasingly offset by compression, so that final pressure increases with increasing Eu .

Trends in mold fill time, shown in Figure 4, are consistent with trends in pressure evolution discussed previously. Specifically, under conditions where compression dominates leakage-induced decay, ($Fr < \approx 10^{-1/2}$), the upward acting pressure force slows the drop's downward motion, leading to increased fill time. Thus, conditions causing cavity pressure to rise above the upper chamber pressure also lengthen fill times (compare Figures 3 and 4). In contrast, when final pressure is less than P_u , inspection of the associated time varying mold pressure (not shown) shows that the pressure force is downward. Since the downward force is proportional to Eu , downward acceleration increases with increasing Eu , leading to increasing compression and decreasing mold fill time. Note too that predicted fill times are consis-

tent with those observed by Watanabe *et al.* in an earlier study of plate mold casting.^[18]

Considering the effect of mold cross-sectional area on mold filling, Figure 5 shows that final mold pressure is less than P_u at all Euler numbers and areas considered. Since P is less P_u , then, as before, and for any given area, the pressure force acts downward with a magnitude that increases with increasing Eu . Thus, compression increasingly offsets pressure decay, resulting in higher final pressures. (Although not shown, compression dominates decay when $Eu = 10^4$, leading to final pressures higher than P_u .) At any given Eu , we observe the intuitively reasonable result that final pressure decreases with increasing cross-sectional area. From Reference 27, it is seen that since $z_c \leq 0$, both the denominator and numerator decrease with increasing A_c ; however, comparing magnitudes of the two terms involving A_c , the term in the numerator is found to be larger. Thus, downward acceleration decreases with increasing \tilde{A}_c , implying less compression relative to decay and lower final pressures. Physically, this is a continuity effect, since gravity and pressure forces do not vary significantly, *i.e.*, by less than an order of magnitude; then, as area increases, given vertical displacements within the crucible produce smaller vertical displacements within the mold. Mold fill times, shown in Figure 6, are again consistent with trends in mold pressure evolution. In particular, since the pressure force is downward under all conditions shown in Figure 5, and since the force magnitude is again proportional to Eu , then for any fixed area, downward acceleration increases, and thus fill time decreases, with increasing Eu . The near-linear increase in fill time with increasing \tilde{A}_c (at fixed Eu) reflects mass conservation. Since forces are relatively fixed, it is found that following a short initial period, the volumetric flow rate from the crucible, Q , remains essentially constant and independent of A_c . Thus, $t_f \approx Q^{-1}A_c$.

Considering finally the effect of loss coefficient, K , on mold filling, we find that trends in final mold pressure and fill time are qualitatively similar to those observed for varying cross-sectional areas. Referring to Figure 7, for example, we see that as K increases at any given Euler number,

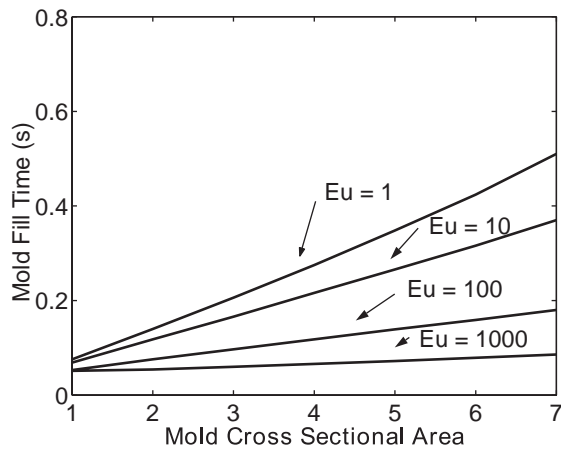


Fig. 6—Effect of dimensionless mold cross-sectional area on dimensional mold fill time. $K = 0.646$, $Fr = 0.254$.

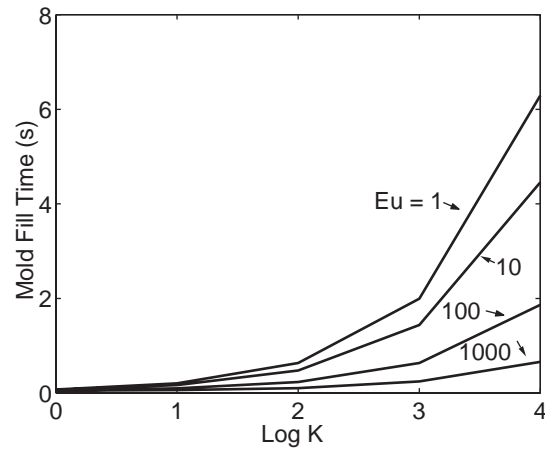


Fig. 8—Effect of pressure loss coefficient on dimensional mold fill time. $Fr = 0.254$, $A_c = 10^{-4} \text{ m}^2$.

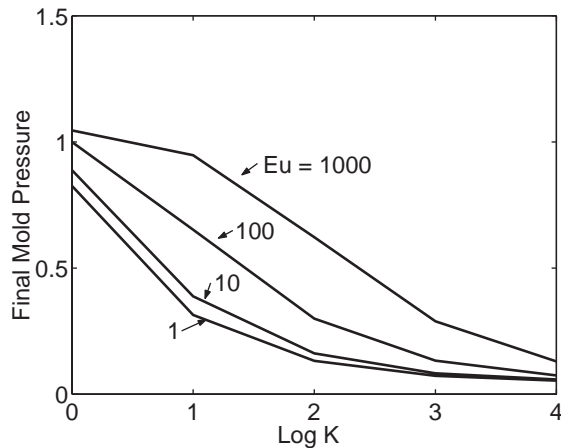


Fig. 7—Effect of pressure loss coefficient on final dimensionless mold pressure. $Fr = 0.254$, $A_c = 10^{-4} \text{ m}^2$.

the final pressure decreases; see Figure 5 for comparison. Similarly, at any given K , final pressure increases with increasing Eu . We can use Eq. [27] and arguments similar to those previously given to explain these results. Likewise, as shown in Figure 8, at fixed Eu , fill time increases with increasing K , similar to the behavior observed for increasing cross-sectional area; refer to Figure 6. Physically, as K increases at any given Euler number, resistance to flow through the crucible's exit also increases. Thus, downward acceleration and gas compression decrease, leading to lower final mold pressures and longer fill times (Figure 8).

V. CONCLUSIONS

Scaling and physical arguments indicate that minimal solidification occurs during mold filling, that frictional effects play a negligible role in drop dynamics, that process gas within the mold remains essentially isothermal, that evaporation recoil is negligible, and that the drop's free surfaces

remain relatively flat during filling. Based on these arguments, a simple energy-based model of the two-chamber pressure casting process is developed. The model is used to examine the effects of various process parameters on casting dynamics. The most important results and observations are as follows.

1. Two competing processes, pressure decay due to gas leakage and compression due to drop motion into the mold, determine mold pressure evolution and consequent mold fill times.
2. When $Fr < \sim 10^{-1/2}$, gravitational forces on the drop are large enough to compress gas within the mold. In this case, the net pressure force on the drop acts upward so that as the Euler number increases at any given Fr , the pressure force also increases, reducing both the drop's downward acceleration and consequent gas compression within the mold. Corresponding mold fill times increase while final mold pressures decrease.
3. When $Fr > \approx 10^{-1/2}$, gravitational forces are no longer large enough for compression to dominate leakage-induced decay. Here, mold pressure drops and remains below its initial magnitude, producing a downward acting pressure force; as the Euler number increases at fixed Fr , the pressure force also increases, increasing both the drop's downward acceleration and gas compression within the mold. Corresponding mold fill times decrease while final pressures increase.
4. Under the reference conditions chosen, and over the range of mold cross-sectional areas examined, $1 \leq \tilde{A}_c \leq 7$, final mold pressure is in every instance less than the upper chamber pressure. Since the pressure force is always downward and is proportional to the Euler number, at any given \tilde{A}_c , drop acceleration and associated gas compression both increase with increasing Eu . Thus, corresponding final mold pressures increase while mold fill times decrease. Since the forces acting on the drop are largely fixed, it is found that the volumetric flow rate from the crucible is likewise fixed. This leads to an essentially linear relationship between mold fill time and \tilde{A}_c .
5. Drop acceleration and associated gas compression decrease with increasing loss coefficient at the crucible

exit. Thus, at fixed Euler number, corresponding final mold pressures decrease while fill times increase.

ACKNOWLEDGMENTS

The authors acknowledge support for this work from NIH/NIDCR Grant No. DE11787. They are also grateful for the editorial assistance with this article from Mrs. Jeanne Santa Cruz.

LIST OF SYMBOLS

A_c	cross-sectional area of mold cavity
A_o	cross-sectional area of crucible exit
A_s	drop's upper free surface area
A_{sp}	characteristic area of contact between drop and crucible
A_u	cross-sectional area of crucible
h_{fg}	latent heat of vaporization
h_{sl}	latent heat of fusion
H_c, L_c	height and width (=depth) of mold cavity
k_g	gas permeability
K	pressure loss coefficient at crucible exit
k_l, k_s	liquid and solid phase thermal conductivities
L_s	crucible height
m	slope of crucible lateral wall
rh_g	gas mass flow rate through bottom of mold
\mathbf{n}, n	unit normal vector and normal direction
P	time-dependent mold pressure
P_c	characteristic pressure on the drop's lower surface
P_o	ambient upper chamber pressure (=P _u)
P_u, P_l	upper and lower chamber pressures
q_p	characteristic drop surface heat flux; characteristic plasma torch flux
Q	volumetric flow rate
R	gas constant for metal evaporate
R_o	crucible exit radius
R_s	characteristic free surface radius of curvature
R_u	crucible top radius
T	temperature
t_d	thickness of mold's bottom wall
t_f	mold fill time
T_g, T_o	process gas temperature
T_m	metal melting temperature
T_b	liquid metal boiling temperature
\mathbf{u}	liquid metal velocity
U_o	liquid metal speed at crucible exit; characteristic axial velocity of crucible
U_s, U_c	velocity of metal drop's upper and lower free surfaces
U_u	characteristic velocity of drop's upper free surface
\mathbf{v}_g	gas velocity within lower mold wall
V	time-dependent gas volume within mold cavity
V_d	metal drop volume
z_s, z_c	axial positions of the drop's upper and lower free surfaces

Greek letters

α_m	metal thermal diffusivity
δ	characteristic viscous boundary layer thickness
δ_s	characteristic solidification thickness
ΔP	pressure difference between upper and lower surfaces
μ_g	process gas viscosity
μ_m	liquid metal viscosity
ν_m	liquid metal kinematic viscosity
ρ_m	liquid metal density
Φ	crucible half angle
σ	liquid metal surface tension
τ	characteristic shear strain at crucible wall
τ_{fill}	characteristic observed mold fill time
τ_o	theoretical characteristic mold fill time

REFERENCES

1. S. Canay, N. Hersek, A. Culha, and S. Bilgic: *J. Oral Rehabil.*, 1998, vol. 25, pp. 759-64.
2. T. Okabe, C. Ohkubo, I. Watanabe, O. Okuno, and Y. Takada: *J. Met.*, 1998, vol. 50, pp. 24-29.
3. H. Her, M. Syverud, and M. Waarli: *Dent. Mater.*, 1993, vol. 9, pp. 15-18.
4. H.S. Al-Mesmar, S.M. Morgano, and L.E. Mark: *J. Prosthet. Dent.*, 1999, vol. 82, pp. 15-21.
5. T. Togaya and K. Ida: *Trans. 3rd World Biomater. Congr.*, 1988, pp. 5p-34, 575.
6. M. Syverud and H. Her: *Dent. Mater.*, 1995, vol. 11, pp. 14-18.
7. Y. Inoue: *J. Jpn. Dent. Mater.*, 1995, vol. 14, pp. 302-12.
8. I. Watanabe, J.H. Watkins, H. Nakajima, M. Atsuta, and T. Okabe: *J. Dent. Res.*, 1997, vol. 76, pp. 773-79.
9. K. Watanabe, S. Okawa, O. Miyakawa, S. Nakano, H. Honnma, N. Shiokawa, and M. Kobayashi: *J. Jpn. Dent. Mater.*, 1993, vol. 12, pp. 496-505.
10. K. Watanabe, S. Okawa, M. Kanatani, T. Okabe, and O. Miyakawa: *J. Jpn. Dent. Mater.*, 1999, vol. 18 (Spec. Iss.), p. 34.
11. S. Mahajan: Ph.D. Dissertation, California Institute of Technology, Pasadena, CA, 1998, pp. 22-89.
12. T. Togaya, S. Tsutsumi, Y. Tani, Y. Yabugami, H. Hiroshima, S. Iwaki, S. Ohyagi, and S. Shimakawa: *Proc. 7th Dental Titanium Conf.*, 1994, pp. 11-12.
13. R.G. Keanini: *Phys. Rev. E*, 1995, vol. 52, pp. 4572-75.
14. P.G. Drazin and W.H. Reid: *Hydrodynamic Stability*, Cambridge University Press, New York, NY, 1981, pp. 19-20.
15. S. Ostrach: *Annual Rev. Fluid Mech.*, Annual Reviews, Palo Alto, CA, 1982, pp. 313-45.
16. X. Zhang and O.A. Basaran: *J. Coll. Interface Sci.*, 1997, vol. 187, pp. 177-78.
17. B. Munson, D. Young, and T. Okiishi: *Fundamentals of Fluid Mechanics*, 3rd ed., Wiley, New York, NY, 1998, pp. 500-01.
18. K. Watanabe, S. Okawa, O. Miyakawa, S. Nakano, N. Shiokawa, and M. Kobayashi: *J. Jpn. Dental Mater. Dev.*, 1991, vol. 10, pp. 77-96.
19. *ASM Handbook, vol. 2, Properties and Selection: Nonferrous Alloys and Special-Purpose Materials*, ASM INTERNATIONAL, Materials Park, OH, 1990, p. 351.
20. K. Watanabe: Niigata University, Niigata, Japan, private communication, 2001.
21. F.P. Incropera and D.P. DeWitt: *Fundamentals of Heat and Mass Transfer*, 4th ed., Wiley, New York, NY, 1996, p. 830.
22. *Physics of Welding*, J.F. Lancaster, ed., Pergamon Press, New York, NY, 1984, p. 112.
23. R.G. Keanini and B. Rubinsky: *Int. J. Heat Mass Transfer*, 1993, vol. 36, pp. 3283-98.